# QUANTUM CHEMICAL AND KINETIC PROPERTIES EVALUATION OF METHYLCHROMENO[2,3-C]PYRAZOL-3(2H)-ONE FOR ALUMINUM CORROSION INHIBITION IN$H_2S0_4$ MEDIUM

.


## *Manuscript Info*

***Manuscript History***
Received: xxxxxxxxxxxxxxx
Final Accepted: xxxxxxxxxxxx
Published: xxxxxxxxxxxxxxx

***Key words:-***
2-methylchromeno[2,3-c]pyrazol-3(2H)-one, Aluminum, Sulfuric acid solution, Gravimetric measurements, Quantum chemical calculations
.



## *Abstract*

Despite its many advantages and good physico-chemical properties, aluminum remains sensitive in certain acidic environments. For this reason, this study evaluates the inhibition efficiency of 2-methylchromeno[2,3-c]pyrazol-3(2H)-one (MCP) on aluminum corrosion in 1 M sulfuric acid solution. Gravimetric measurements were combined with quantum chemical calculations to analyze its anticorrosive behavior. These calculations were based on Density Functional Theory (DFT) in basis set 6-31G(d,p) with B3LYP functional.The results show that inhibition efficiency increases with concentration and immersion time, reaching 92.87% at 298 K for 5 mM, while increasing temperature reduces inhibition efficiency. The increase in activation energy in the presence of 2-methylchromeno[2,3-c]pyrazol-3(2H)-one confirms the predominance of physisorption, corroborated by activation enthalpy and entropy values, indicating endothermic dissolution with increased disorder. Theoretical calculations reveal that MCP's strong inhibition activity is linked to its ability to give up and accept electrons, favouring its adsorption by physico-chemical interactions dominated by electrostatic forces. Experimental and theoretical approaches converge perfectly, confirming that the inhibitor used is promising for the protection of aluminum in acidic media at low temperatures. These results open up prospects for its use in real-life industrial conditions, and for the development of more effective anticorrosive strategies.






## Introduction:-

The industrial revolution, which continues to spread throughout the world, brings both benefits and negative impacts on the environment. Many industries use metals that are frequently exposed to aggressive environments, making them vulnerable to corrosion [1]. Metal corrosion, and aluminum corrosion in particular, is a major industrial and economic problem. Although aluminum is renowned for its natural resistance to oxidation, thanks to the spontaneous formation of a protective alumina layer, this barrier becomes unstable in highly acidic environments [2], particularly sulfuric acid. Under such conditions, aluminum undergoes accelerated degradation, resulting in material losses, reduced mechanical performance and higher maintenance costs [3]. To mitigate the deleterious effects of this degradation, the use of corrosion inhibitors has emerged as an effective, simple and economically viable strategy [4]. Among these, organic inhibitors are attracting growing interest due to their ability to adsorb onto the metal surface via their heteroatoms (O, N, S) and conjugated π-systems, thus forming a protective film capable of reducing corrosive attack [5]. However, the choice of a high-performance inhibitor relies not only on its experimental efficacy, but also on an understanding of its electronic properties and kinetic behavior vis-à-vis adsorption and dissolution mechanisms [6]. At present, organic inhibitors that are accessible and have low toxicity are preferred. In this context, pyrazoles and their derivatives stand out for their low toxicity, conjugated structure and

ability to interact effectively with metal surfaces [7]. Furthermore, in order to design more effective organic inhibitors, numerous studies have turned to quantum chemistry to establish precise correlations between the molecular properties of compounds and their inhibitory capacity [8,9]. The molecular structure, including electronic distribution, electron density of active sites and frontier molecular orbitals, as well as various electronic parameters can be determined by theoretical calculations [10]. This information not only makes it possible to predict the activity of an inhibitor on the metal surface, but also to better understand the adsorption mechanisms and evaluate the relative efficacy of different compounds, paving the way for rational design of more selective and effective inhibitors.

Within this framework, the main objective of the present study is to evaluate the anticorrosive properties of the compound 2-methylchromeno[2,3-c]pyrazol-3(2H)-one in the prevention of aluminum corrosion in 1 M sulfuric acid solution.

## Material And Methods:-

### Chemicals used:

The inhibitor used is 2-methylchromeno[2,3-c]pyrazol-3(2H)-one (MCP). It was synthesized and characterized by a team at Laboratory Organic Chemistry and Natural Synthesis of Félix Houphouët Boigny University, Cocody (Côte d'Ivoire). The molecular formula of this inhibitor is C11H8N2O2 with a molar mass M = 200.05 g/mol. Its molecular structure is shown in Figure 1.

**Figure 1**. Molecular structure of 2-methylchromeno[2,3-c]pyrazol-3(2H)-one (MCP)

An acetone solution with purity P = 99.5%, density d = 0.79 and molar mass M = 58.08 $g.mol^{-1}$ was used to remove all traces of grease and native oxide from each aluminum sample. A sulfuric acid solution with purity P = 98%, density d = 1.84 and molar mass M = 98.08 $g.mol^{-1}$ was used to prepare a 1M concentration solution. This solution was used as a blank for all gravimetric tests.

### Gravimetric measurements:

Samples of 99%-pure aluminum in the form of cylindrical rods 10mm high and 25mm in diameter were polished with abrasive papers of successively finer grain sizes down to 800 grit, then thoroughly rinsed in distilled water. They were then washed in an acetone solution to remove all traces of oxide, before being dried in an oven at 80°C for 10 minutes. Each sample thus treated was weighed on a high-precision balance (± 0.1 mg), then immersed in 50 mL of a 1 M sulfuric acid solution, in the absence of inhibitor. The initial mass recorded ($m_1$) was then compared with that measured after a one-hour immersion in the sulfuric acid solution, this time containing the corrosion inhibitor. After this treatment, the samples were carefully rinsed, dried

and weighed again to obtain the final mass ($m_2$). Mass loss ($\Delta m = m_1 - m_2$) was calculated by averaging three trials carried out under the same experimental conditions. To study the influence of immersion time we maintained the temperature at 298K and while keeping the same MCP concentrations, mass losses were evaluated for 4h, 6h, 8h and 24h. From these data, the average corrosion rate (W), the rate of coverage of the metal surface by the inhibitor (θ), and the inhibition efficiency (EI%) were calculated as a function of temperature and the concentration of inhibitor used. The following expressions were used to determine these corrosion parameters

$$W = \frac{m_1 - m_2}{S_e.t} = \frac{\Delta m}{S_e.t} \quad (1)$$

$$IE(\%) = \frac{W_0 - W}{W_0} * 100 \quad (2)$$

$W_0$and $W$ (expressed in g.cm$^{-2}$.h$^{-1}$) are respectively the corrosion rate in the absence and presence of MCP, $S_e$ is the total surface area of aluminum sample and $t$ is the immersion time.

**Quantum chemical calculations:**

To establish a correlation between experimental data and MCP's quantum chemistry parameters, its geometry was first optimized using Gaussview 5.0 computer graphics software. This optimization was carried out using B3LYP correlation exchange functional, in 6-31G(d, p) basis set [11,12](Figure 2). This basis set enabled precise geometry and electronic properties to be obtained for a wider range of organic compounds. Global molecular descriptor calculations were performed using Gaussian 09 software [13]. Thus, quantum chemical parameters such as highest occupied molecular orbital energy ($E_{HOMO}$), lowest unoccupied molecular orbital energy ($E_{LUMO}$), energy gap (ΔE), dipole moment (μ), ionization energy ($I$), electron, affinity ($A$), electronegativity (χ), global hardness (η), global softness ($\sigma$), electrophylicity index (ω),fraction of electrons transferred ($\Delta N$) andtotal energy ($E_T$) were calculated. The expressions below, derived from conceptual DFT, are used to calculate the quantum descriptors [14,15,16].

$$I = -E_{HOMO} \quad (3)$$

$$A = -E_{LUMO} \quad (4)$$

$$\Delta E = E_{LUMO} - E_{HOMO} \quad (5)$$

$$\mu_P = \left(\frac{\partial E}{\partial N}\right)_{v(r)} = -\chi \quad (6)$$

$$\chi = \frac{I+A}{2} \quad (7)$$

$$\sigma = \frac{1}{\eta} = \frac{2}{I-A} \quad (8)$$

$$\eta = \frac{I-A}{2} \quad (9)$$

$$\omega = \frac{\mu_P^2}{2\eta} = \frac{(I+A)^2}{4(I-A)} \quad (10)$$

$$\Delta N = \frac{\phi_{Al} - \chi_i}{2(\eta_{Al} + \eta_i)} \quad (11)$$

For calculations the theoretical values of$\phi_{Al} = 4.28\ eV$ [17]and hardness $\eta_{Al} = 0$ [17]have been used for aluminum.

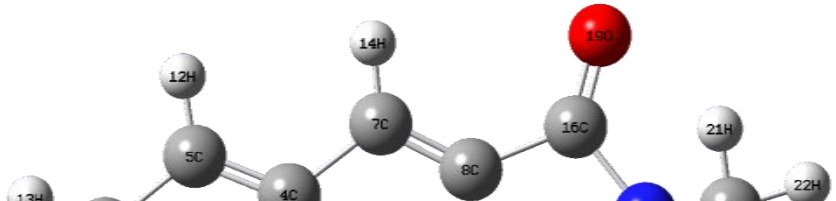

**Figure 2**. Optimized structure of 2-methylchromeno[2,3-c]pyrazol-3(2H)-one

## Results And Discussion:-

### Effect of temperature and concentration:

To assess the influence of temperature and inhibitor concentration, the inhibitory efficacy values determined under different experimental conditions were plotted as a function of these two parameters (Figure 3). This allows us to visualize the evolution of efficacy as a function of inhibitor concentration at various temperatures, and conversely to appreciate the effect of temperature variation for a given concentration.

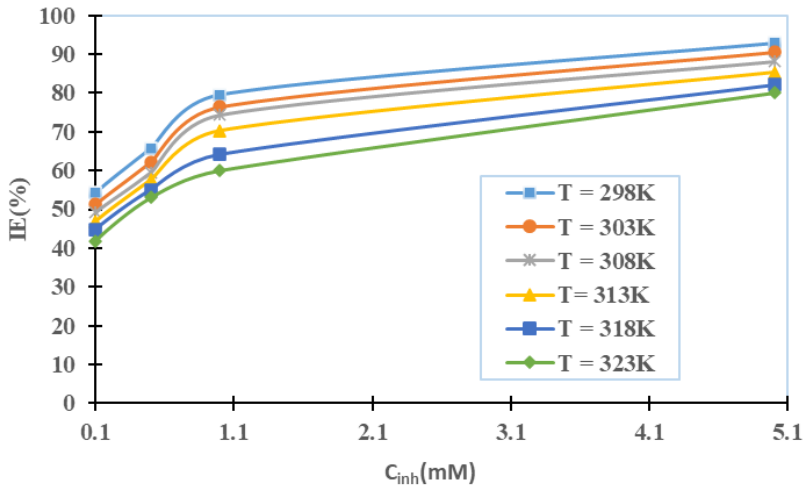


**Figure 3**. Evolution de l'efficacité inhibitrice en fonction de la concentrationet de la température

The experimental curves show an upward trend in inhibitory efficacy as a function of MCP concentration. Examination of the figure clearly shows that the effectiveness of this compound increases with increasing concentration, while it tends to decrease with increasing temperature. The maximum value recorded is 92.87% at 298 K.

MCP's inhibitory action can be explained by the adsorption of its molecules on the aluminum surface. This adsorption limits dissolution of the metal substrate and reduces its mass loss. The improvement in efficiency with increasing concentration results from the progressive covering of the surface by the inhibitor molecules. The presence of heteroatoms (N, O), combined with the aromatic character and electron density of its π systems, favors the formation of a stable protective film. This acts as a physical barrier, increasing in thickness and compactness in proportion to the concentration of MCP, thus hindering the corrosion process.

On the other hand, higher temperatures lead to a decrease in inhibitory efficiency. This can be attributed to the partial desorption of adsorbed molecules, or to the increased corrosive activity of the medium, which accentuates metal dissolution. As a result, the protective layer formed becomes less and less effective, and aluminum mass loss increases.

These observations are in line with results reported in previous work[18,19], confirming that the behavior of MCP follows the trend generally observed for organic inhibitors acting by adsorption.

**Immersion time effect:**

Figure 4 shows the evolution of inhibition efficiency as a function of immersion time.

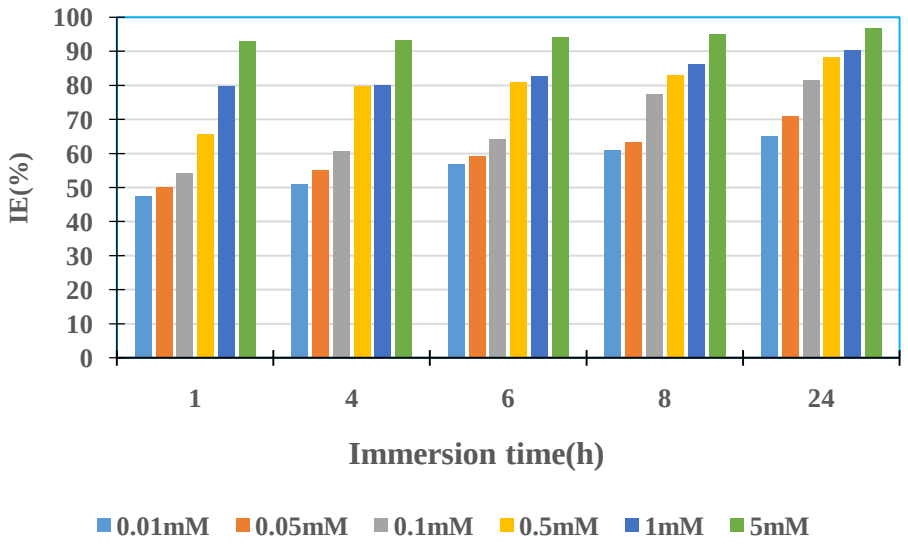

**Figure 4.** Evolution of inhibition efficiency as a function of immersion time and concentration

Figure 4 shows the evolution of inhibitory efficacy as a function of MCP concentration and immersion time. Each colored band illustrates the response corresponding to a given inhibitor concentration. Analysis of the graph shows a progressive increase in inhibitory efficacy as MCP concentration and immersion time increase. These results show that the higher the concentration of MCP and the longer the contact time with the metal surface, the greater the inhibitory effect. In particular, after 24 hours of immersion, the efficacy measured is slightly higher than that observed for shorter durations (1 h, 4 h, 6 h and 8 h). This suggests that longer immersion times promote a more complete and stable adsorption process of MCP molecules to the aluminum surface. Nevertheless, it is important to note that the one-hour duration is still sufficient to significantly reveal the molecule's inhibitory properties. All the observations reveal a progressive and reinforced attachment of MCP to the metal substrate, leading to the formation of a protective barrier that limits the corrosive attack of the sulfuric medium. This behavior confirms MCP's role as an effective inhibitor of aluminum corrosion, and underlines its ability to stabilize its effectiveness under prolonged exposure conditions.

**Activation parameters analysis:**

**Activation energy:**

The relationship between temperature and metal corrosion rate is based on the Arrhenius-type relationship. It is expressed as follows [20].

$$W = Aexp(-\frac{E_a}{RT}) \qquad (12)$$

Using the relation $logW = logA - \frac{E_a}{2.3.R.T}$, Figure 5 shows the evolution of $logW$ as a function of $\frac{1}{T}$. Activation energy values are determined from the slopes of the straight lines obtained, and are given in Table 1.

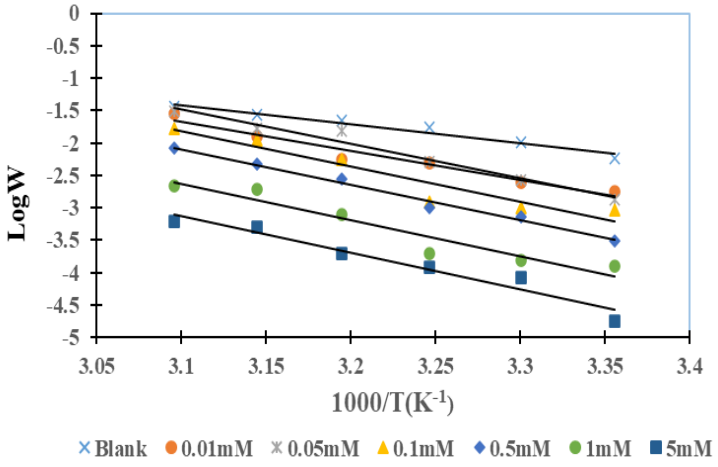

**Figure 5.** $logW$ Versus $\frac{1}{T}$ .

**Table 1.** Activation Energy value

| $C_{inh}(mM)$ | Equations | $E_a(kJmol^{-1})$ |
|---|---|---|
| 0 | $logW = -2.954 * \frac{1}{T} + 7.7481$ | 56.60147584 |
| 0.01 | $logW = -4.5116 * \frac{1}{T} + 12.314$ | 86.44658714 |
| 0.05 | $logW = -5.3333 * \frac{1}{T} + 15.052$ | 102.191148 |
| 0.1 | $logW = -5.4824 * \frac{1}{T} + 15.183$ | 105.0480471 |
| 0.5 | $logW = -5.5071 * \frac{1}{T} + 14.98$ | 105.5213228 |
| 1 | $logW = -5.5514 * \frac{1}{T} + 14.58$ | 106.3701533 |
| 5 | $logW = -5.6562 * \frac{1}{T} + 14.408$ | 108.378222 |

The straight lines show that the corrosion rate increases as the temperature of the reaction medium rises. This rate is much higher in the absence (control) of the inhibitor. The values of activation energy ($E_a$)increase with increasing inhibitor concentration. This analysis shows that the presence of MCP increases activation energy required to dissolve the metal. The adsorption of its molecules onto metal surface requires significant energy, reflecting a blocking of active sites that requires a greater energy input. This rise in $E_a$accounts for the slowdown in the dissolution process in MCP presence, a slowdown that is all the more marked the higher the inhibitor concentration [20].

The activation energy values measured in the presence of MCP are significantly higher than those obtained in its absence. This suggests that MCP is adsorbed onto metal substrate via electrostatic bonds. However, these interactions, which are weak and sensitive to temperature variations, do not provide effective corrosion inhibition at high temperatures. Thus, the poor inhibiting performance observed at high temperatures is due to the physiosorbed nature of the interaction between the MCP and the metal surface [21].

**Enthalpy and entropy of Activation:**

Enthalpy variations($\Delta H_a^*$)and entropy ($\Delta S_a^*$)were determined from the alternative formula of Arrhenius equation:

$$log(\frac{W}{T}) = log(\frac{R}{\aleph.h}) + \frac{\Delta S_a^*}{2{,}3.R} - \frac{\Delta H_a^*}{2.3.R.T} \qquad (13)$$

Where A: Pre-exponential factor ; W : Corrosion rate, R : Perfect gas constant; T : absolute temperature; $\aleph$ : Avogadro number; h : Planck's constant;

Figure 6 shows the evolution of $log(\frac{W}{T})$ depending on $\frac{1}{T}$. The slopes and intercepts of the lines obtained were used to determine these activation quantities. Table 2 shows the characteristics of the lines obtained and the values of $\Delta H_a^*$ et $\Delta S_a^*$.

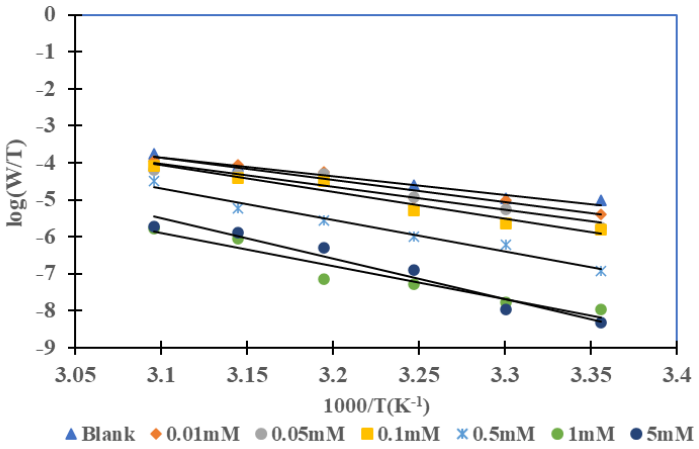


**Figure 6.** $log(\frac{W}{T})$ Versus $\frac{1}{T}$.

The values of activation enthalpy ($\Delta H_a^*$). are positive and increase with increasing MCP concentration. The positive enthalpy reflects the endothermic nature of aluminum dissolution process in sulfuric acid solution [22]. In addition, the high, positive values of activation entropy ($\Delta S_a^*$) indicate that the kinetically decisive step is associated more with a dissociation phenomenon than with an association mechanism [23,24]. This positive entropy reflects an increase in disorder during the transformation of reactants into the activated complex. This increased disorder results from the desorption of species initially attached to aluminum surface, progressively replaced by water molecules already present in the reaction medium.

**Tableau 2**. Values ofenthalpy ($\Delta H_a^*$). and entropy($\Delta S_a^*$)

| $C_{inh}(mM)$ | Equations | $\Delta H_a^*(kJmol^{-1})$ | $\Delta S_a^*(Jmol^{-1}K^{-1})$ |
|---|---|---|---|
| 0 | $logW = -5.007 * \frac{1}{T} + 11.668$ | 95.93892672 | 25.795328 |
| 0.01 | $logW = -5.9614 * \frac{1}{T} + 14.609$ | 114.2261469 | 82.074304 |
| 0.05 | $logW = -6.2186 * \frac{1}{T} + 15.258$ | 119.1543459 | 94.493568 |
| 0.1 | $logW = -7.1841 * \frac{1}{T} + 18.202$ | 137.6542527 | 150.829952 |
| 0.5 | $logW = -8.5199 * \frac{1}{T} + 21.728$ | 163.2494631 | 218.303488 |
| 1 | $logW = -8.9259 * \frac{1}{T} + 21.775$ | 171.0288129 | 219.20288 |
| 5 | $logW = -10.978 * \frac{1}{T} + 28.54$ | 210.3490189 | 348.65792 |

**Quantum chemical properties of the inhibitor:**

**Global reactivity:**

The quantum chemical properties of the inhibitor are based on the global reactivity quantum chemical parameters. These parameters were calculated using DFT and are shown in Table 3.

**Table 3.** Global reactivity parameters

| Quantum descriptors of global reactivity | Valeurs |
|---|---|
| $E_{HOMO}$ (eV) | -5.5474 |
| $E_{LUMO}$ (eV) | -2.6281 |
| Energy Gap ΔE (eV) | 2.9193 |
| dipole momentμ (D) | 3.5516 |
| ionization energyI (eV) | 5.5474 |
| Electron, affinity A (eV) | 2.6281 |
| Electronegativityχ (eV) | 4.0878 |
| Global hardnessη (eV) | 1.4597 |
| Global softness ($\sigma$) $(eV)^{-1}$ | 0.6851 |
| Fraction of electrons transferredΔN | 0.0658 |
| Electrophylicity indexω | 5.7240 |
| Total energy $E_T$(Ha) | -683.6605 |

In light of previous work [25,26] the values obtained for highest occupied molecular orbital energy ($E_{HOMO}$) and that of lowest unoccupied molecular orbital energy ($E_{LUMO}$) are found to be high and low respectively. These characteristics indicate that the molecule studied has a strong ability to give up and take up electrons from aluminum. This dual ability favors covalent bonds formation between inhibitor and metal, facilitating its adsorption onto surface and leading a protective film formation. This acts as an insulating barrier to aggressive environment. This observation confirms the link between the high inhibition efficiency recorded at low temperatures and the molecule's ability to act as both electron donor and electron acceptor. Furthermore, energy gap
$\Delta E = E_{LUMO} - E_{HOMO}$ constitutes a key parameter of molecular reactivity: the smaller this gap, the more reactive [27,28]. Thus, the low value of ΔE obtained for MCP reflects a high reactivity, consistent with its experimentally demonstrated inhibition efficiency.
With regard to dipole moment (μ), the literature is divided on its role in predicting inhibition efficiency [29,30]. Some authors note no clear correlation between μ and anticorrosive action, while others consider that a low value of the dipole moment would favor adsorption of the molecule and, consequently, its protective efficacy [31,32 ]. The results of the present study seem to agree with the latter hypothesis, suggesting that a reduced dipole moment facilitates the accumulation of MCP on metal surface and enhances its inhibition power.
A comparison of electronegativities shows that of aluminum (4.28 eV) is higher than that of MCP (4.0878 eV), resulting in a positive fraction of electrons transferred (ΔN). This transfer of electrons from the molecule to metal helps compensate for the electron deficit caused by aggressive ions from sulfuric acid.
Finally, a study of electronic distributions of HOMO and LUMO orbitals (Figure 7) reveals that

they are mainly located around nitrogen (N) and oxygen (O) atoms, as well as in aromatic regions. The mapping shows that the positive phase of the orbitals is represented by color red, while negative phase appears in green.

The red/green areas show HOMO and LUMO electronic distributions within the molecule. The electronic distributions of the highest occupied molecular orbital (HOMO) highlight localized areas on nitrogen (N) and oxygen (O) atoms, as well as on aromatic rings. This distribution suggests that these sites are the main centers of electron donation onto metal surface. Similarly, the regions associated with the lowest unoccupied molecular orbital (LUMO) also appear on aromatic rings and on the same heteroatoms, reflecting the molecule's ability to accept electrons from the metal and establish covalent bonds. These results indicate that interaction between MCP molecule and the metal surface occurs preferentially at sites enriched in π electron density.

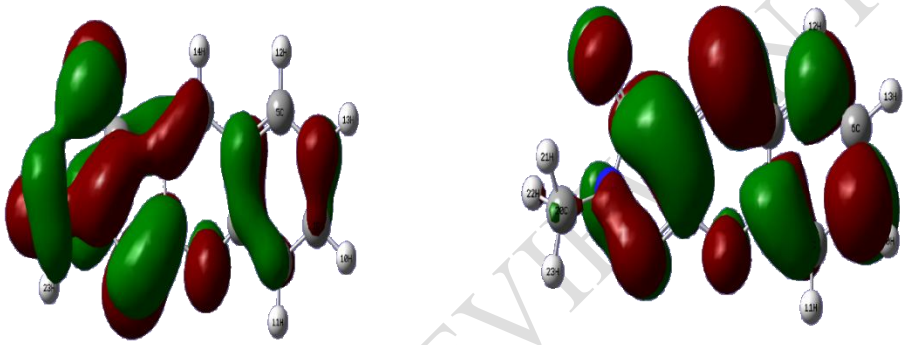

HO BV

**Figure 7**. Orbitales HO et BV

**Identifying sites of local reactivity:**

Active sites were identified using Fukui and dual descriptor functions.

The following formulas are used to determine these local reactivity parameters [32-35]:

- Nucleophilic attack $f_k^+ = q_k(N+1) - q_k(N)$ (14)
- Electrophilic attack $f_k^- = q_k(N) - q_k(N-1)$ (15)
- Dual descriptor $\Delta f_k(\mathrm{r}) = f_k^+ - f_k^-$ (16)

Where$q_k(N+1)$, $q_k(N)$ et $q_k(N-1)$are the electronic population of atomic sites k in $(N+1)$, $N$ and $(N-1)$ electronic systems

The values of these local reactivity chemical quantum parameters are listed in Table 4.

These values include both positive and negative values. According to previous studies, the highest positive value of $f_k^+$ and $\Delta f_k(\mathrm{r})$ indicates the most likely site for nucleophilic attacks [34]. For the molecule studied, carbon C(20) is therefore the most likely site for nucleophilic attack. In this case, C(20) carbon is a zone ready to receive electrons from the metal. While a higher value $f_k^-$ and the lowest value of $\Delta f_k(\mathrm{r})$ identifies the most likely site for electrophilic attack. C(9) atom is then the most likely site for electrophilic attack. This site is the zone that supplies electrons to metal.

**Table 4**. Mulliken atomic charges and local reactivity quantum parameters

| Atom | $q_k(N+1)$ | $q_k(N)$ | $q_k(N-1)$ | $f_k^+$ | $f_k^-$ | $\Delta f_k$(r) |
|---|---|---|---|---|---|---|
| 1 C | -0.007634 | -0.076945 | 0.143311 | 0.069311 | -0.220256 | 0.289567 |
| 2 C | 0.011242 | -0.159172 | -0.03122 | 0.170414 | -0.127952 | 0.298366 |
| 3 C | -0.005409 | 0.339114 | 0.04238 | -0.344523 | 0.296734 | -0.641257 |
| 4 C | 0.003203 | 0.074489 | -0.06016 | -0.071286 | 0.134649 | -0.205935 |
| 5 C | -0.005173 | -0.154381 | 0.192107 | 0.149208 | -0.346488 | 0.495696 |
| 6 C | 0.007202 | -0.088839 | -0.072796 | 0.096041 | -0.016043 | 0.112084 |
| 7 C | -0.011997 | -0.102503 | 0.396382 | 0.090506 | -0.498885 | 0.589391 |
| 8 C | -0.000342 | 0.015038 | 0.048092 | -0.01538 | -0.033054 | 0.017674 |
| **9 C** | 0.029219 | 0.553039 | 0.010143 | -0.52382 | **0.542896** | **-1.066716** |
| 10 H | 0.000275 | 0.108887 | -0.007338 | -0.108612 | 0.116225 | -0.224837 |
| 11 H | -0.000466 | 0.119505 | 0.000852 | -0.119971 | 0.118653 | -0.238624 |
| 12 H | 0.000222 | 0.109886 | -0.009021 | -0.109664 | 0.118907 | -0.228571 |
| 13 H | -0.000286 | 0.103358 | 0.002476 | -0.103644 | 0.100882 | -0.204526 |
| 14 H | 0.000451 | 0.135906 | -0.018103 | -0.135455 | 0.154009 | -0.289464 |
| 15 O | 0.01853 | -0.5595 | 0.013716 | 0.57803 | -0.573216 | 1.151246 |
| 16 C | 0.004862 | 0.558213 | 0.144803 | -0.553351 | 0.41341 | -0.966761 |
| 17 N | 0.020691 | -0.326793 | 0.096373 | 0.347484 | -0.423166 | 0.77065 |
| 18 N | 0.173387 | -0.371898 | -0.027181 | 0.545285 | -0.344717 | 0.890002 |
| 19 O | 0.040142 | -0.512522 | 0.11831 | 0,552664 | -0,630832 | 1,183496 |
| **20 C** | 0.758347 | -0.452087 | 0,042464 | **1.210434** | -0.494551 | **1.704985** |
| 21 H | -0.013917 | 0.20862 | -0.004673 | -0.222537 | 0.213293 | -0.43583 |
| 22 H | -0.00632 | 0.241832 | -0.018799 | -0.248152 | 0.260631 | -0.508783 |
| 23 H | -0.01623 | 0.236756 | -0.002119 | -0.252986 | 0.238875 | -0.491861 |

**Inhibition mechanism:**

MCP mechanism inhibition of aluminum corrosion in $H_2SO_4$ ,1M can be explained as follows. MCP compound is protonated in sulfuric acid solution, and the protonated species will be in equilibrium with its corresponding neutral phase according to the following equation:

$$2MCP + H_2SO_4 \rightleftarrows 2[MCPH]^+ + SO_4^{2-} \qquad (17)$$

The protonated form of the inhibitor interacts with the negatively charged aluminum surface, due to the prior adsorption of sulfate ions ($SO_4^{2-}$) from sulfuric acid. This interaction promotes a protective film formation stabilized by electrostatic forces between the ionic species of inhibitor and sulfate ions, reflecting a physisorption mechanism. On the other hand, the inhibitor is also adsorbed by donor-acceptor interactions, involving the free doublets of heteroatoms as well as π-electrons of aromatic rings. This mode of interaction, associated with a charge transfer between molecule and metal, corresponds to a chemisorption process. The study of electronic parameters such as the number of electrons transferred (ΔN), the energies $E_{HOMO}$, $E_{LUMO}$, as well as energy gap (ΔE) confirms this second type of adsorption. The inhibition mechanism is summarized in Figure 8.

The green line indicates chemisorption, while the red broken line shows the electrostatic

interaction between the sulfate ion and the cationic form of MCP (physisorption).

## Conclusions:-

The study carried out on 2-methylchromeno[2,3-c]pyrazol-3(2H)-one (MCP) highlighted its notable effectiveness as an aluminum corrosion inhibitor in a 1 M sulfuric acid medium. Experimental results from gravimetric measurements showed that the inhibition efficiency of MCP increased with concentration and immersion time, reaching a maximum value of 92.87% at 298 K for 5 mM, while decreasing with increasing temperature. Analysis of the activation parameters confirmed the predominance of a physisorption mechanism, supported by an endothermic process accompanied by an increase in disorder. Quantum-chemical calculations carried out within DFT framework highlighted MCP's dual ability to give up and accept electrons, a property that favors its interaction with the metal surface via physico-chemical adsorption. The identification of active sites showed that heteroatoms (O, N) and aromatic rings constitute the main centers of reactivity, playing a key role in the formation of a protective film on aluminum.The convergence of experimental and theoretical data confirms that MCP is a promising organic inhibitor, capable of effectively limiting aluminum corrosion in acidic media at moderate temperatures. These results pave the way for the potential use of MCP in industrial applications, while suggesting that future work could explore its behavior under real-life conditions, as well as its synergy with other inhibitors.

## References:


[1] Nnabuk O. E., Momoh-Yahaya, H and Emeka E. O. (2015). Theoretical and experimental studies on the corrosion inhibition potentials of some purines for aluminum in 0.1M HCl, *Journal of Advanced Research*,6(2):203-217.

[2] Shuduan, D. and Xianghong L. Inhibition by Jasminum Shuduan, D.and Xianghong, L,(2012). Inhibition by Jasminum nudiflorum Lindl. leaves extract of the corrosion of aluminium in HCl solution. *Corrosion Science*,64:253-262

[3] Bochuan, T., Anqing, F., Lei, G., Yun, R., Junle, X.and Riadh, M., Wenpo, L.(2023). Insight into anti-corrosion mechanism of Dalbergia odorifera leaves extract as a biodegradable inhibitor for X70 steel in sulfuric acid medium. *Industrial Crops and Products*, 194:116106

[4] Shawky, M. H., Elawady Y.A., Ahmed A.I.and Baghlaf A.O. (1979). Studies on the inhibition of aluminium dissolution by some hydrazine derivatives, *Corrosion Science*,19(12): 951-959

[5] Rajeev, K. G., Manisha, M., Chandrabhan, V. and Quraishi, M.A.(2017).Aminoazobenzene and diaminoazobenzene functionalized graphene oxides as novel class of corrosion inhibitors for mild steel: Experimental and DFT studies,*Materials Chemistry and Physics*, 198: 360-373.

[6] Chandrabhan, V., Eno, E. E., Quraishi, M. A., Chaudhery, M. H. (2021). Recent developments in sustainable corrosion inhibitors: design, performance and industrial scale applications, *Materials Advances*,2(12): 3806-3850).

[7] Dereli, Ö.(2016). Molecular structure and spectral (FT-IR, Raman) investigations of 3-aminocoumarin. *Optics and Spectroscopy*, 120: 690–700.

[8] Mustafa, R., Albayati, S. K., Necmi, D. Savaş, K., Riadh, M., Hassane, L., Rachid, S., Ismat, H. A., Majed, M. A.and Ill-Min, C.(2020).Synthesis, crystal structure, Hirshfeld surface analysis and DFT calculations of 2-[(2,3-dimethylphenyl)amino]-N'-[(E)-thiophen-2-ylmethylidene]benzohydrazide.*Journal of Molecular Structure*,1205:127654

[9] Wei, L., Qingyun, L., Xue, R., Wenpo, L., Bochuan, T., Anqing, F., Shengtao, Z.(2021), A new pyridazine derivative synthesized as an efficient corrosion inhibitor for copper in sulfuric acid medium: Experimental and theoretical calculation studies.*Journal of Molecular Liquids*,341:117370.

[10] Adejoro, I.A., Akintayo, D.C.and Ibeji C.U. (2016). The efficiency of chloroquine as corrosion inhibitor for aluminium in 1M HCl solution: Experimental and DFT study. *Jordan Journal of Chemistry*, 11(1): 38–49.

[11] Lee, C., Yang W and Parr R.G. (1988). Development of the Colle-Salvetti Correlation-Energy Formula into a Functional of the Electron Density. *Physical Review B,* 37: 785–789.

[12] Becke, A.D. (1993). Density-Functional Thermochemistry. III. The Role of Exact Exchange. *Journal of Chemical Physics,* 98: 1372–1377.

[13] Frisch M.J., Trucks G.W., Schlegel H.B., Scuseria G.E., Robb M.A., & Cheeseman J.R. (2009). Gaussian 09.

[14] Arafat, T., Omar, K. A., Ahmed, F., Ayman, M. M., Ahmed, Eldesoky M and Ahmed A. F. (2024). Effect of Adsorption and Interactions of New Triazole-Thione-Schiff Bases on the Corrosion Rate of Carbon Steel in 1 M HCl Solution: Theoretical and Experimental Evaluation ACS Omega , 2024 9 (6): 6761-6772.

[15] Toghan, A., Fawzy, A., Alakhras, A.I., Alqarni, N.; Zaki, M.E.A., Sanad, M.M.S., Farag, A.A.(2023) Experimental Exploration, RSM Modeling, and DFT/MD Simulations of the Anticorrosion Performance of Naturally Occurring Amygdalin and Raffinose for Aluminum in NaOH Solution. Coatings, 13: 704.

[16] Mohamed, E. A., Altalhi, A. A., Amer, A., Negm, N. A., Azmy, E. A. M., & Farag, A. A. (2023). Two novel Schiff bases derived from 3-amino-1,2,4-triazole as corrosion inhibitors for carbon steel pipelines during acidizing treatment of oil wells: Laboratory and theoretical studies. Energy Sources, Part A: Recovery, Utilization, and Environmental Effects, 45(2): 3246–3265.

[17] Pearson RG.(1988). Absolute Electronegativity and Hardness:application to Inorganic Chemistry, Inorganic Chemistry,27(4): 734-740.

[18] Beda, R.H.B., Niamien, P.M., Avo Bilé E.B., & Trokourey A. (2017). Inhibition of aluminum corrosion in 1.0 M HCl by caffeine: Experimental and DFT studies. Advances in Chemistry, Hindawi, Article ID 6975248.

[19] Rokia T.H., Tigori M.A., Koffi A.A., & Niamien P.M. (2024). Exploring the anticorrosion performance of 2-(((4-chlorobenzyl)thiol)methyl)-1H-benzo[d]imidazole on aluminum in 1 M HNO3. Journal of Scientific Research, 16(3): 899–915.

[20] Jmiai, A.,Tara,S, El Issami,M., Hilali,O., Jbara,L.and Bazzi. (2021). A new trend in corrosion protection of copper in acidic medium by using Jujube shell extract as an effective green and environmentally safe corrosion inhibitor: Experimental, quantum chemistry approach and Monte Carlo simulation study,Journal of Molecular Liquids. Journal of Molecular Liquids, 322, 114509.

[21] Umoren, S.A., Obot, I.B.and Ebenso, E.E. (2008). Corrosion inhibition of aluminium using exudate gum from Pachylobus edulis in the presence of halide ions in HCl. Journal of Chemistry, 5(2): 355.

[22] Desai, P.S.and Desai, F.P. (2023). An overview of sustainable green inhibitors for aluminum in acid media. AIMS Environmental Science, 10(1): 33–62.

[23] Desai, K.C., Desai, P.S.,Adarsh, Patel, M and Bhumika B. (2024). Caesalpinia crista seed

is used as an eco-friendly inhibitor to prevent the corrosion of aluminium in hydrochloric acid solutions. Chemistry of Inorganic Materials, 4: 100067.

[24] Yeo , M., Niamien, P. M., Bilé E. B. A.and Trokourey, A. (2018). Thiamine hydrochloride as a potential inhibitor for aluminium corrosion in 1.0 M HCl: Mass Loss and DFT Studies. Journal of Computational Methods in Molecular Design, 8 :13–25.

[25] Ammouchi, N., Allal, H., Belhocine, Y., Bettaz, S and Zouaoui E. (2020). DFT computations and molecular dynamics investigations on conformers of some pyrazinamide derivatives as corrosion inhibitors for aluminum. Journal of Molecular Liquids, 300: 112309.

[26] Eddy, N.O., Momoh-Yahaya, H.and Oguzie, E.E. (2015). Theoretical and experimental studies on the corrosion inhibition potentials of some purines for aluminum in 0.1 M HCl. Journal of Advanced Research, 6(2): 203–217.

[27] Kumar, D., Jain, V .and Rai B. (2020). Imidazole derivatives as corrosion inhibitors for copper: A DFT and reactive force field study. Corrosion Science, 171: 108724.

[28] Benhiba, F., Sebbar, N.K., Bourazmi, H., Belghiti, M.E., Hsissou, R.and Hökelek T. (2021). Corrosion inhibition performance of 4-(prop-2-ynyl)-[1,4]-benzothiazin-3-one against mild steel in 1 M HCl solution: Experimental and theoretical studies. International Journal of Hydrogen Energy, 46(51): 25800–25818.

[29] Sahin, M., Gece G., Karei, F.and Bilgic S. (2008). Experimental and theoretical study of the effect of some heterocyclic compounds on the corrosion of low carbon steel in 3.5% NaCl medium. Journal of Applied Electrochemistry, 38(1): 809–815.

[30] Wazzan, N.A., Obot, I.B.and Kaya S. (2016). Theoretical modeling and molecular level insights into the corrosion inhibition activity of 2-amino-1,3,4-thiadiazole and its 5-alkyl derivatives. Journal of Molecular Liquids, 221: 579–602

[31] Khaled K.F. (2008). Molecular simulation, quantum chemical calculations and electrochemical studies for inhibition of mild steel by triazoles. Electrochimica Acta, 53(9): 3484–3492.

[32] Zhang, J., Li, W., Zuo X., Chen Y., Luo, W and Zhang Y. (2021). Combining experiment and theory researches to insight into anti-corrosion nature of a novel thiazole derivatives. Journal of the Taiwan Institute of Chemical Engineers, 122: 190–200.

[33] Martínez-Araya, J.I. (2015). Why is the dual descriptor a more accurate local reactivity descriptor than Fukui functions. Journal of Mathematical Chemistry, 5: 451–465

[34] Morell, C., Grand A.and Toro-Labbé A. (2005). New dual descriptor for chemical reactivity. Journal of Physical Chemistry A, 109: 205–212.

[35] Damej, M., Kaya S., EL Ibrahimi, B., Lee, H.S., Molhi A. and Serdaroğlu G. (2021). The corrosion inhibition and adsorption behavior of mercaptobenzimidazole and bis-mercaptobenzimidazole on carbon steel in 1.0 M HCl: Experimental and computational insights. Surfaces and Interfaces, 24: 101095.